Multi-target Range and Angle detection for MIMO-FMCW radar with limited antennas

Himali Singh and Arpan Chattopadhyay

Abstract—**Multiple-input multiple-output (MIMO) radar has several advantages with respect to the traditional radar array systems in terms of performance and flexibility. However, in order to achieve high angular resolution, a MIMO radar requires a large number of antenna elements, which increases hardware design and computational complexities. Although spatial compressive sensing (CS) has been recently considered for a pulsed-waveform MIMO radar with sparse random arrays, such methods for the frequency-modulated continuous wave (FMCW) radar remain largely unexplored. In this context, we propose a novel multi-target localization algorithm in the range-angle domain for a MIMO FMCW radar with a sparse array of randomly placed transmit/ receive elements. In particular, we first obtain the targets' range-delays using a discrete Fourier transform (DFT)-based focusing operation. The target angles are then recovered at each detected range using CS-based techniques exploiting the sparsity of the target scene. Our simulation results demonstrate the effectiveness of the proposed algorithm over the classical methods in detecting multiple targets with a sparse array.**

Index Terms—**Compressive sensing, FMCW-MIMO radar, random arrays, range-angle estimation, sparse arrays.**

I. Introduction

Frequency-modulated continuous wave (FMCW) radars have become a popular choice for short-range applications like automotive radars [1, 2], human vital sign monitoring [3], synthetic aperture radars (SARs) [4], and surveillance systems [5]. The main advantages of FMCW radar are portability, low cost, and high resolution. An FMCW radar transmits a finite train of (piece-wise) linear frequency-modulated (LFM) chirps in each coherent processing interval (CPI). The target returns are mixed with the transmitted signal at the receiver to obtain a complex sinusoidal intermediate frequency (IF) signal. The targets' locations (and velocities if moving) information can be extracted from the frequencies of this IF signal. To this end, fast Fourier transforms (FFTs) have traditionally been used to estimate these frequencies [1]. However, to localize targets in the angular domain, multiple transmit and receive antennas are required. In MIMO radars, multiple orthogonal waveforms are transmitted simultaneously with the target returns processed jointly by the multiple receive antennas. The MIMO radar achieves a better angular resolution than conventional radar by exploiting a large number of degrees of freedom of a virtual array synthesized with a small number of physical antenna elements. In this work, we focus on multi-target range-angle detection using MIMO FMCW radars. Conventionally, frequency estimation algorithms like 2D-FFT [6], 2D-MUSIC [7], and ESPRIT [8] are used to estimate both targets' ranges and angles of arrival (AOAs) from the received signal.

From the array processing theory, it is known that a high angular resolution requires a large array aperture with a large number of antenna elements to avoid ambiguities in angle estimation [9]. Although MIMO technology helps to achieve higher resolution, the cost of synthesizing a large virtual array with the half-wavelength element spacing (spatial Nyquist sampling rate) can be very high. In this context, sparse linear arrays (SLAs) have been proposed recently for both pulsed-waveform and continuous-wave radars [6, 10, 11]. Optimal sparse array design was considered in [12] while [6] designed a non-uniform SLA and applied digital beamforming techniques for AOA estimation after interpolating for the missing measurements in the synthesized SLA. On the other hand, [11] suggested matrix completion techniques to complete the corresponding linear array for angle detection.

Compressed sensing (CS) addresses sparse signal recovery with fewer measurements [13]. The sparse array setup enables spatial compressive sensing such that the CS recovery naturally suits our target localization problem. Note that the target scene is sparse since only a small number of targets are present in the scene. The CS-recovery-based localization has recently been applied for angle estimation for pulsed-MIMO radar [10]. In [14], CS-based algorithms were used to process measurements from a traditional full array. Besides spatial compression, CS techniques have also been considered in radars for reduced sampling rate [15, 16], interference mitigation [17], and multi-target shadowing effect mitigation in constant false-alarm rate (CFAR) detection [18].

Contributions: In this paper, we present a novel multi-target localization algorithm to detect targets' ranges and AOAs using a random SLA. Prior CS-based methods (e.g. [10]) often address only angle detection at a known range bin. Here, we consider both range and angle detection in a MIMO FMCW radar. For range detection, we exploit a discrete Fourier transform (DFT)-based focusing operation followed by binary integration [9] of measurements across pulses and virtual array channels, trading off range resolution for higher detection probability. For angle recovery, we use

The authors are with the Electrical Engineering department, Indian Institute of Technology (IIT) Delhi. A.C. is also associated with Bharti School of Telecommunications Technology and Management, IIT Delhi. Email: {eez208426, arpanc}@ee.iitd.ac.in.

A. C. acknowledges support via the professional development fund and professional development allowance from IIT Delhi, grant no. GP/2021/ISSC/022 from I-Hub Foundation for Cobotics and grant no. CRG/2022/003707 from Science and Engineering Research Board (SERB), India. H. S. acknowledges support via Prime Minister Research Fellowship.

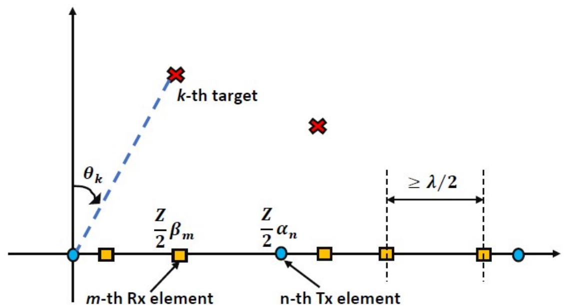

Fig. 1. MIMO radar system (□ and ∘ denote receivers and transmitters, respectively).

CS-based techniques reducing the number of antenna elements needed to attain performance comparable to that of a full array. Finally, our numerical simulations illustrate the proposed method's performance compared to classical-FFT processing.

II. Radar System model

Consider a colocated MIMO radar system, as shown in Fig. 1, composed of N_T transmitters and N_R receivers forming a (possibly overlapping) array of total aperture Z_T and Z_R, respectively, and define $Z \doteq Z_T + Z_R$. The n-th transmitter's and m-th receiver's locations along the x-axis are $Z\alpha_n/2$ and $Z\beta_m/2$, respectively, where $\alpha_n \in [-Z_T/Z, Z_T/Z]$ and $\beta_m \in [-Z_R/Z, Z_R/Z]$. Note that α_n and β_m are randomly drawn from appropriate uniform distributions [10]. The transmitters transmit LFM chirps, orthogonal across transmitters. Consider f_c as the carrier frequency and γ as the chirp rate of the LFM chirp of duration T. The FMCW radar's transmitted chirp is modeled as $s(\bar{t}) = \exp\left(j2\pi\left(f_c\bar{t} + \frac{\gamma}{2}\bar{t}^2\right)\right)$ for $0 \leq \bar{t} \leq T$, with $\bar{t}$ as the continuous-time index. A total of P chirps is transmitted in each CPI. Different orthogonal waveform designs for MIMO-FMCW radar transmitters have been proposed in [19, 20]. For simplicity, we consider time-domain multiplexing, where the transmitters transmit the same signal with relative time shifts. In our proposed detection algorithm, we process each transmitted chirp independently and use binary integration [9] after detection across pulses (in a CPI) to obtain the estimated ranges. On the contrary, classical-FFT processing considers coherent or non-coherent integration of the pulses to average out the interference and noise before detection [9]. In Section IV, we discuss how binary integration improves the detection probability over classical processing. Similarly, the orthogonality of the transmitted signals allows the corresponding received signal components to be separated at each receiver. Hence, we first focus on the received signal component at the m-th receiver due to the single chirp transmitted from the n-th transmitter.

We assume a target scene of K stationary, far-field, non-fluctuating point targets. We denote the k-th target's range and angle of arrival (AOA) as R_k and θ_k, respectively. Denote $\tau_{m,n,k}$ as the total time-delay in the k-th target's return at the m-th receiver from the n-th transmitted signal such that the received signal component is given as $r_{m,n}(\bar{t}) = \sum_{k=1}^{K} a_k s(\bar{t} - \tau_{m,n,k})$, where a_k is the complex amplitude proportional to the k-th target's radar cross-section (RCS). The time delay $\tau_{m,n,k}$ consists of the range delay τ_k^R and angular delay $\tau_{m,n,k}^{\theta}$ as

$$\tau_{m,n,k} = \tau_k^R + \tau_{m,n,k}^{\theta}, \tag{1}$$

where $\tau_k^R = 2R_k/c$ and $\tau_{m,n,k}^{\theta} = Z(\alpha_n + \beta_m)\sin(\theta_k)/2c$ with constant c denoting the speed of light. Note that the far-field assumption leads to a constant AOA across the array.

Unlike a pulsed radar system, an FMCW radar first mixes the m-th received signal with the n-th transmitted signal to obtain IF signal $y_{m,n}(\bar{t})$ as $y_{m,n}(\bar{t}) = \sum_{k=1}^{K} a_k^* \exp\left(j2\pi\left(\gamma\tau_{m,n,k}\bar{t} + f_c\tau_{m,n,k} - \frac{\gamma}{2}\tau_{m,n,k}^2\right)\right) + w_{m,n}(\bar{t})$, where $(\cdot)^*$ represents the conjugate operation and $w_{m,n}(\bar{t})$ is the interference plus-noise term. Each IF signal $y_{m,n}(\bar{t})$ is sampled at sampling frequency f_s as $y_{m,n}[t] = \sum_{k=1}^{K} a_k^* \exp\left(j2\pi\left(\gamma\tau_{m,n,k}\frac{t}{f_s} + f_c\tau_{m,n,k} - \frac{\gamma}{2}\tau_{m,n,k}^2\right)\right) + w_{m,n}[t]$, for $0 \leq t \leq N-1$, where $N = f_sT$ is the total number of samples in a single pulse and $w_{m,n}[t]$ is the sampled noise. Here, we represent the discrete-time index by t. For the N_T transmitters and N_R receivers MIMO setup, we obtain 'N_TN_R' sampled measurements $\{y_{m,n}[t]\}_{1\leq m\leq N_R, 1\leq n\leq N_T}$ for all P pulses.

III. Sparse array Recovery algorithm

The spatial compressive sensing framework proposed in [10] for pulsed MIMO radar assumes an independent range-Doppler processing and focus only on targets in a given range-Doppler bin for AOA estimation. On the contrary, here, we consider both range and AOA detection. In Section III-A, we adopt a DFT-focusing operation to estimate the targets' ranges and separate the range and AOA information. Finally, in Section III-B, the CS-based recovery provides the AOA estimates at each detected range bin.

A. Range detection

Consider the N-point DFT $Y_{m,n}[l] = \sum_{t=0}^{N-1} y_{m,n}[t]\exp(-j2\pi lt/N)$ of IF signal $y_{m,n}[t]$ as

$$Y_{m,n}[l] = \sum_{k=1}^{K} a_k^* \exp\left(j2\pi\left(f_c\tau_{m,n,k} - \frac{\gamma}{2}\tau_{m,n,k}^2\right)\right) \times \sum_{t=0}^{N-1} \exp\left(j2\pi\left(\frac{\gamma\tau_{m,n,k}}{f_s} - \frac{l}{N}\right)t\right) + W_{m,n}[l], \tag{2}$$

for $0 \leq l \leq N-1$, where $W_{m,n}[l] = \sum_{t=0}^{N-1} w_{m,n}[t]\exp(-j2\pi lt/N)$ represents the noise term.

Replacing $N = f_sT$, we first analyze the sum of exponents $\sum_{t=0}^{N-1} \exp\left(j\left(\frac{2\pi\gamma}{f_s}\right)\left(\tau_{m,n,k} - \frac{l}{\gamma T}\right)t\right)$ in (2). Consider the sum of M exponents $g(x|\overline{x}) = \sum_{q=0}^{M-1} e^{j(x-\overline{x})q\omega}$ for given constants $\overline{x}$ and ω. We can approximate $|g(x|\overline{x})| \approx M$ for $|x-\overline{x}| \leq \pi/M\omega$, and 0 otherwise. The approximation implies that in the focus zone $|x-\overline{x}| \leq \pi/M\omega$, the M exponents are coherently integrated while the signal outside the focus zone is severely attenuated. In [15], this focusing approximation was introduced as Doppler focusing across pulses to reduce the joint delay-Doppler estimation problem to delay only estimation at a particular Doppler frequency. In our case, the sum of exponents appears naturally in the DFT of $y_{m,n}[t]$.

Using the focusing approximation for the sum of N exponents (indexed by t) in (2), we have

$$Y_{m,n}[l] \approx \sum_{k'=1}^{K'} a_{k'}^* N \exp\left(j2\pi\left(f_c\tau_{m,n,k'} - \frac{\gamma}{2}\tau_{m,n,k'}^2\right)\right) + W_{m,n}[l], \tag{3}$$

where $\{a_{k'}, \tau_{m,n,k'}\}_{1\leq k'\leq K'}$ represents the subset of targets which satisfy $|\tau_{m,n,k'} - l/(\gamma T)| \leq 1/(2\gamma T)$ for the given l-th DFT bin. Assuming $\tau_k^R \gg \tau_{m,n,k}^\theta$ for all targets, we have $\tau_{m,n,k'} \approx \tau_{k'}^R$ such that the received signal from targets at ranges satisfying $|\tau_{k'}^R - l/(\gamma T)| \leq 1/(2\gamma T)$ are coherently integrated, resulting in a (magnitude) peak at the l-th DFT bin. Furthermore, the practical values of γ and T for an FMCW radar ensures that the value $1/(2\gamma T)$ is small enough and $\tau_{k'}^R \approx l/(\gamma T)$. Hence, using threshold detection to identify the peaks in $Y_{m,n}[l]$ (corrupted by noise), we obtain the range estimate R' corresponding to a DFT peak at l'-th bin as $R' = \frac{cl'}{2\gamma T}$. These range estimates are computed independently for all P pulses and for all $N_T N_R$ measurements $\{y_{m,n}[t]\}_{1\leq m\leq N_R, 1\leq n\leq N_T}$. The detected ranges are first filtered for false alarms across the P pulses using binary integration, i.e., only the ranges detected in majority of pulses are considered valid target ranges. Similarly, the detected ranges are also filtered across the $N_T N_R$ measurements.

The classical-FFT range processing also involves threshold detection for peaks in the IF signal's DFT. However, in classical processing, all the pulses are processed together non-coherently, which increases the DFT's frequency resolution and hence, the range resolution. Contrarily, we trade off range resolution by processing each pulse independently for reduced missed detection probability. In particular, in the case of close-range targets, the classical-FFT often suffers from false peaks dominating the actual target peaks. Using binary integration across pulses and the virtual array channels, the detection probability is enhanced with a constant false alarm probability, which is further discussed in Section IV-A with a simulated example of three close-range targets. However, the CS-based angle detection procedure developed in the following section can also be applied to non-coherently processed pulses.

B. Angle detection

Consider a detected range bin at the l'-th DFT point. Substituting (1) in (3) for $\tau_{m,n,k'}$, we obtain $Y_{m,n}[l'] = W_{m,n}[l'] + \sum_{k'=1}^{K'} a_{k'}^* N \exp\left(j2\pi\left(f_c\tau_{k'}^R - \frac{\gamma}{2}(\tau_{k'}^R)^2\right)\right) \times \exp\left(j2\pi(f_c - \gamma\tau_{k'}^R)\tau_{m,n,k'}^\theta\right)$, using $(\tau_{k'}^R)^2 \gg (\tau_{m,n,k'}^\theta)^2$. For practical FMCW radars, carrier frequency f_c (in GHz), chirp rate γ (in MHz/μs) and short-range delay τ_k^R (a few μs) are such that the term $\gamma\tau_{k'}^R$ is negligible and

$$Y_{m,n}[l'] = \sum_{k'=1}^{K'} a_{k'}^* N \exp\left(j2\pi\left(f_c\tau_{k'}^R - \frac{\gamma}{2}(\tau_{k'}^R)^2\right)\right) \times \exp\left(j2\pi f_c\tau_{m,n,k'}^\theta\right) + W_{m,n}[l']. \tag{4}$$

Note that the exponential terms with the range and angle delays are now separated in $Y_{m,n}[l']$.

Denote $x_k \doteq a_k^* N \exp\left(j2\pi\left(f_c\tau_k^R - \frac{\gamma}{2}(\tau_k^R)^2\right)\right)$, and $Y_{m,n}^p[l']$ as the l'-th DFT coefficient computed for the p-th pulse. Stack the measurements $Y_{m,n}^p[l']$ for all (m,n)-pairs in a $N_T N_R \times 1$ vector $\mathbf{y}_p$. Now, define the '$N_T N_R \times P$' matrix $\mathbf{Y} = [\mathbf{y}_1, \ldots, \mathbf{y}_P]$. Similarly, define the $K' \times P$ matrix $\widetilde{\mathbf{X}} = [\widetilde{\mathbf{x}}_1, \ldots, \widetilde{\mathbf{x}}_P]$ with $\widetilde{\mathbf{x}}_p = [x_1, \ldots, x_{K'}]^T$. Now, substituting $\tau_{m,n,k}^\theta = Z(\alpha_n + \beta_m)\sin(\theta_k)/2c$ in (4) yields

$$\mathbf{Y} = \widetilde{\mathbf{C}}(\boldsymbol{\theta})\widetilde{\mathbf{X}} + \mathbf{W}, \tag{5}$$

where the $N_T N_R \times K'$ matrix $\widetilde{\mathbf{C}}(\boldsymbol{\theta}) = [\mathbf{c}(\theta_1), \ldots, \mathbf{c}(\theta_{K'})]$ with each column $\mathbf{c}(\theta) = [\exp(j\pi f_c Z(\alpha_1 + \beta_1)sin(\theta)), \ldots, \exp(j\pi f_c Z(\alpha_{N_T} + \beta_{N_R})sin(\theta))]^T$, known as the virtual array steering vector [10] parameterized by the AOA θ. Here, $\mathbf{W}$ represents the $N_T N_R \times P$ stacked noise matrix.

We aim to recover $\boldsymbol{\theta}$ and $\widetilde{\mathbf{X}}$ from $\mathbf{Y}$ with a small number of antenna elements exploiting the target scene's sparseness. Assume a grid of G points $\boldsymbol{\phi}_{1\leq g\leq G}$ of the possible target AOAs θ with $G \gg K$ and negligible discretization errors. Each grid element ϕ_g parameterizes a column of $\widetilde{\mathbf{C}}(\boldsymbol{\theta})$. Hence, we can define a $N_T N_R \times G$ dictionary matrix $\mathbf{C} = [\mathbf{c}(\phi_1), \ldots, \mathbf{c}(\phi_G)]$. From (5), the measurements $\mathbf{Y}$ become

$$\mathbf{Y} = \mathbf{C}\mathbf{X} + \mathbf{W}, \tag{6}$$

where the unknown $G \times P$ matrix $\mathbf{X}$ contains the target AOAs and complex amplitudes (x_k). A non-zero row of $\mathbf{X}$ represents a target present at the corresponding grid point. Hence, the system (6) is sparse since $\mathbf{X}$ has only $K' \ll G$ non-zero rows. Given the measurements $\mathbf{Y}$ and matrix $\mathbf{C}$, AOA estimation reduces to determining the support (non-zero rows) of $\mathbf{X}$. Note that the matrix $\mathbf{C}$ and hence, the recovery guarantees depend on the choice of grid points $\boldsymbol{\phi}_{1\leq g\leq G}$ as well as the number and (random) positions of the transmitters and receivers ($\{\alpha_n\}_{1\leq n\leq N_T}$ and $\{\beta_m\}_{1\leq m\leq N_R}$). In [10], authors also discuss the sufficient conditions on the grid and the random array for high probability recovery.

We consider CS-based algorithms to recover sparse matrix $\mathbf{X}$ with limited antenna elements. CS problems can be classified as single measurement vector (SMV) models for $P = 1$ where $\mathbf{Y}$ reduces to a single vector, or multiple measurement vector (MMV) models for $P \geq 1$. Our problem (6) is an MMV setting. However, we first consider the SMV setting with $P = 1$ such that $\mathbf{Y} = \mathbf{y}$, $\mathbf{X} = \mathbf{x}$ and $\mathbf{W} = \mathbf{w}$ in (6). Recovering a sparse $\mathbf{x}$ from $N_T N_R$ measurements $\mathbf{y}$ involves solving the computationally expensive non-convex combinatorial l_0-norm problem $\min_{\mathbf{x}} \|\mathbf{x}\|_0$ s.t. $\|\mathbf{y} - \mathbf{C}\mathbf{x}\|_2 \leq \nu$, where parameter ν is chosen based on the noise level $\|\mathbf{w}\|_2$ or the sparsity of $\mathbf{x}$. In practice, an approximate solution is obtained using polynomial-complexity matching pursuit (MP) or basis pursuit (BP) algorithms. In Section IV-B, we consider orthogonal MP (OMP) [21] and simultaneous OMP (SOMP) [22], respectively, for the sparse recovery in SMV and MMV settings.

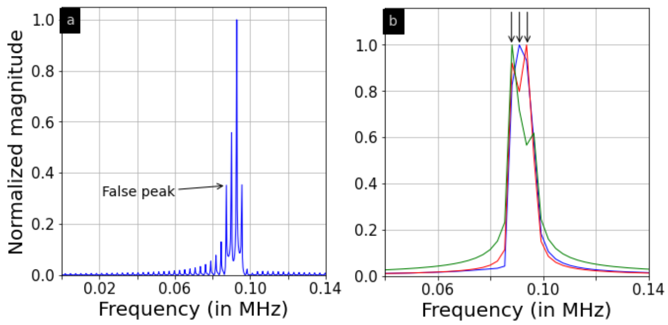

Fig. 2. DFT for (a) Classical range-FFT; and (b) Three different pulses for the proposed method (arrows indicate the detected peaks).

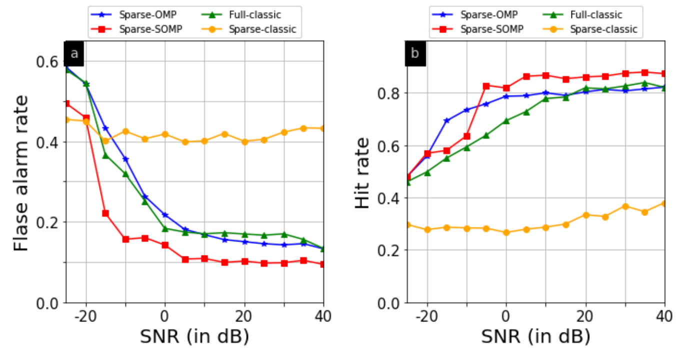

Fig. 3. Average (a) false alarm rate, and (b) hit rate at different SNRs for classical-FFT processing and the proposed method.

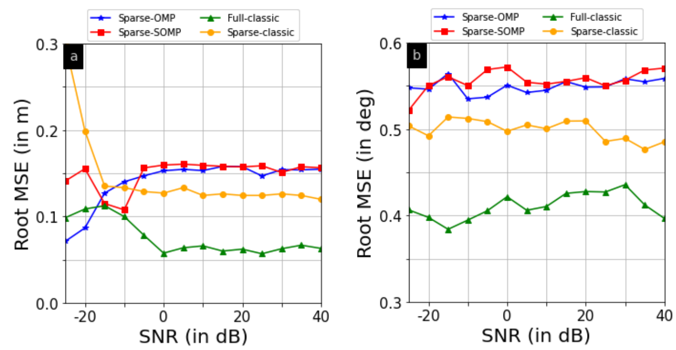

Fig. 4. Root MSE in (a) range, and (b) angle estimation at different SNRs for classical-FFT processing and the proposed method.

IV. Simulation Results

We now demonstrate the performance of the proposed method in comparison to the classical FFT-processing. In Section IV-A, we first investigate the effect of binary integration for range processing discussed in Section III-A. The simulation results for a sparse target scene are provided in Section IV-B.

We considered a MIMO-FMCW radar system transmitting at $f_c = 9.4$ GHz. The transmitted bandwidth was chosen as $B = 250$ MHz with $T = 363\mu$s (chirp rate $\gamma = B/T$) and sampling frequency $f_s = 1.4$ MHz such that the range resolution was 0.6 m. One CPI consisted of $P = 10$ MIMO sweeps. For the sparse array, 3 transmitters and 3 receivers (total 6 antenna elements) were placed uniformly over the array apertures $Z_T = Z_R = 6\lambda$, where λ is the wavelength of the transmitted signal. Note that in this case $\alpha_n, \beta_m \in [-0.5, 0.5]$ for $1 \leq n, m \leq 3$. For the full array, we considered 4 transmitters and 8 receivers with two transmitters placed on either side of the array with λ spacing and the receivers placed in the middle with 0.5λ and 0.25λ spacings between the receivers and closest transmitter-receiver elements, respectively [7]. This arrangement results in a virtual array of 20 unique 0.5λ-separated elements. The target gains were generated as $a_k = \exp(j\psi_k)$ with ψ_k drawn from i.i.d. uniform distribution over $[0, 2\pi)$. Noise $w_{m,n}[t]$ is assumed i.i.d. zero-mean complex circular Gaussian $\mathcal{CN}(0, \sigma^2\mathbf{I})$, mutually independent across pulses and virtual array channels such that the signal-to-noise ratio (SNR) is $-10\log_{10}(\sigma^2)$ [10].

A. DFT processing: classical and proposed method

Consider three close-range targets with ranges $R_1 = 20.6$ m, $R_2 = 20.0$ m and $R_3 = 19.4$ m at AOAs $\theta_1 = \theta_2 = \theta_3 = 0°$ in the noise-free case. Fig. 2a shows the range-FFT computed in the classical-FFT processing. Fig. 2b shows the DFT computed in the proposed method for three different pulses from measurement $y_{1,1}[t]$. We observe that non-coherent pulses processing in the classical method provides a refined spectrum compared to the proposed method of processing one pulse at a time. However, the classical range-FFT suffers from the side-lobe effect resulting in a false peak of the same order as the third target (R_3) peak such that reducing the false alarms results in a missed detection. On the other hand, using the binary integration method, the missed targets in one pulse can be detected at other pulses (or some other $y_{m,n}[t]$ measurement), which enhances the detection probability by trading off range resolution.

B. Performance analysis

We considered $K = 5$ targets with target delays and AOAs chosen uniformly at random with ranges in $[10m, 40m]$ and AOAs in $[-15°, 15°]$, such that we have close-range targets as well as multiple targets at the same range. For CS-based angle recovery, we considered OMP with the vector measurement $\mathbf{y}$ as the sum across 10 pulses and SOMP for matrix measurement $\mathbf{Y}$. In [10], authors assumed a known sparsity level and used the prior information of the actual number of targets K in the CS algorithms. However, here, we assumed a sparsity of $K_{max} = 10$ for OMP and SOMP algorithms. The target AOAs were then obtained using threshold detection on the recovered signal. Hence, we do not require a prior estimate of K. The grid $\phi_{1\leq g\leq G}$ was chosen as 150 uniformly spaced points in the $\sin(\theta)$ domain in the interval $[-0.7071, 0.7071]$. Note that similar to the classical processing, the AOA estimates are uniform in the $\sin(\theta)$ domain.

We consider hit rate and root-mean-squared error (RMSE) of the recovered targets as the performance metrics. A 'hit' is defined as a range-angle estimate within 0.6 m in range and $1°$

in angle of the true target. The recovery error is computed for the estimates classified as hits. We vary the thresholds of the threshold detectors to maintain a constant false-alarm rate at different SNRs. The hit rate and false alarm rate for different SNRs, averaged over 300 independent simulations, are shown in Fig. 3 for the proposed method and classical-FFT processing for both full and sparse arrays. The corresponding range and angle recovery errors are shown in Fig. 4.

From Fig. 3, we observe that for high SNRs, the proposed OMP-based method for the sparse array attains the same performance as the classical method for the full array, but with only half the number of antenna elements. On the other hand, reducing the antenna elements drastically degrades the classical-FFT's performance. The hit rate of the classical processing (full array) at lower SNRs reduces due to the side-lobe effect discussed earlier while at high SNRs, the false peaks from the side lobes are not prominent. On the contrary, the proposed method maintains the same hit rate for different SNRs. The SOMP-based recovery further increases the proposed method's detection probability with a reduced false alarm rate compared to OMP. SOMP improves the detection ability by exploiting the correlation among the measurements across different pulses to recover the true target AOAs. In Fig. 4a, we observe that the classical method has a lower range recovery error for both full and sparse arrays, because of its refined range FFT. The proposed method achieves a slightly higher range error of 0.15 m. Similarly, in Fig. 4b, the classical method slightly outperforms the proposed method in terms of angle recovery error. However, the classical method's angular resolution (hence, the error) depends on the array aperture. A higher angular resolution requires an increase in the array aperture and the number of antenna elements. Contrarily, the proposed method's angular resolution depends on the grid points G such that the angle recovery error can be reduced with a finer grid $\phi_{1\leq g\leq G}$. However, the number and locations of the antenna elements still affect the dictionary matrix $\mathbf{C}$, which determines the CS-based algorithms' recovery probability.

V. Summary

We have proposed a novel CS-based multi-target detection algorithm in the range-angle domain for MIMO FMCW radar. The proposed method enables a random array MIMO system to localize multiple targets with reduced number of antenna elements. For range detection, we considered a DFT-based focusing operation with binary integration across pulses and virtual array channels, for reduced missed detection probability. Finally, the SMV and MMV-based CS recovery algorithms provide the AOAs estimates. Our numerical experiments suggest that the proposed method can achieve the traditional full-array hit rate with limited antenna elements. Furthermore, the MMV-based angle recovery can outperform both SMV-based and classical-FFT methods.

References

[1] S. Sun, A. P. Petropulu, and H. V. Poor, "MIMO radar for advanced driver-assistance systems and autonomous driving: Advantages and challenges," *IEEE Signal Processing Magazine*, vol. 37, no. 4, pp. 98–117, 2020.

[2] S. M. Patole, M. Torlak, D. Wang, and M. Ali, "Automotive radars: A review of signal processing techniques," *IEEE Signal Processing Magazine*, vol. 34, no. 2, pp. 22–35, 2017.

[3] Z. Xu, C. Shi, T. Zhang, S. Li, Y. Yuan, C.-T. M. Wu, Y. Chen, and A. Petropulu, "Simultaneous monitoring of multiple people's vital sign leveraging a single phased-MIMO radar," *IEEE Journal of Electromagnetics, RF and Microwaves in Medicine and Biology*, vol. 6, no. 3, pp. 311–320, 2022.

[4] A. Meta, P. Hoogeboom, and L. P. Ligthart, "Signal processing for FMCW SAR," *IEEE Transactions on Geoscience and Remote Sensing*, vol. 45, no. 11, pp. 3519–3532, 2007.

[5] S. Saponara and B. Neri, "Radar sensor signal acquisition and multidimensional FFT processing for surveillance applications in transport systems," *IEEE Transactions on Instrumentation and Measurement*, vol. 66, no. 4, pp. 604–615, 2017.

[6] R. Feger, C. Wagner, S. Schuster, S. Scheiblhofer, H. Jager, and A. Stelzer, "A 77-GHz FMCW MIMO radar based on an SiGe single-chip transceiver," *IEEE Transactions on Microwave theory and Techniques*, vol. 57, no. 5, pp. 1020–1035, 2009.

[7] F. Belfiori, W. van Rossum, and P. Hoogeboom, "2D-MUSIC technique applied to a coherent FMCW MIMO radar," in *IET International Conference on Radar Systems (Radar 2012)*, 2012, pp. 1–6.

[8] A. N. Lemma, A.-J. Van Der Veen, and E. F. Deprettere, "Analysis of joint angle-frequency estimation using ESPRIT," *IEEE Transactions on Signal Processing*, vol. 51, no. 5, pp. 1264–1283, 2003.

[9] M. A. Richards, *Fundamentals of radar signal processing*. McGraw-Hill Education, 2014.

[10] M. Rossi, A. M. Haimovich, and Y. C. Eldar, "Spatial compressive sensing for MIMO radar," *IEEE Transactions on Signal Processing*, vol. 62, no. 2, pp. 419–430, 2013.

[11] S. Sun and A. P. Petropulu, "A sparse linear array approach in automotive radars using matrix completion," in *IEEE International Conference on Acoustics, Speech and Signal Processing (ICASSP)*. IEEE, 2020, pp. 8614–8618.

[12] K. Diamantaras, Z. Xu, and A. Petropulu, "Sparse antenna array design for MIMO radar using softmax selection," *arXiv preprint arXiv:2102.05092*, 2021.

[13] M. Elad, *Sparse and redundant representations: from theory to applications in signal and image processing*. Springer, 2010, vol. 2, no. 1.

[14] C. Alistarh, L. Anitori, W. L. van Rossum, S. K. Podilchak, J. Thompson, and M. Sellathurai, "Compressed Sensing for MIMO Radar using SIW Antennas for High Resolution Detection," in *2021 18th European Radar Conference (EuRAD)*. IEEE, 2021, pp. 485–488.

[15] O. Bar-Ilan and Y. C. Eldar, "Sub-Nyquist radar via Doppler focusing," *IEEE Transactions on Signal Processing*, vol. 62, no. 7, pp. 1796–1811, 2014.

[16] Y. Yu, A. P. Petropulu, and H. V. Poor, "MIMO radar using compressive sampling," *IEEE Journal of Selected Topics in Signal Processing*, vol. 4, no. 1, pp. 146–163, 2010.

[17] A. Correas-Serrano and M. A. Gonzalez-Huici, "Sparse reconstruction of chirplets for automotive FMCW radar interference mitigation," in *2019 IEEE MTT-S International Conference on Microwaves for Intelligent Mobility (ICMIM)*, 2019, pp. 1–4.

[18] Z. Cao, J. Li, C. Song, Z. Xu, and X. Wang, "Compressed sensing-based multitarget CFAR detection algorithm for FMCW radar," *IEEE Transactions on Geoscience and Remote Sensing*, vol. 59, no. 11, pp. 9160–9172, 2021.

[19] J. De Wit, W. Van Rossum, and A. De Jong, *Orthogonal waveforms for FMCW MIMO radar*. IEEE, 2011.

[20] G. Babur, O. A. Krasnov, A. Yarovoy, and P. Aubry, "Nearly orthogonal waveforms for MIMO FMCW radar," *IEEE Transactions on Aerospace and Electronic Systems*, vol. 49, no. 3, pp. 1426–1437, 2013.

[21] Y. C. Pati, R. Rezaiifar, and P. S. Krishnaprasad, "Orthogonal matching pursuit: Recursive function approximation with applications to wavelet decomposition," in *Proceedings of 27th Asilomar conference on Signals, Systems and Computers*. IEEE, 1993, pp. 40–44.

[22] J. A. Tropp, A. C. Gilbert, and M. J. Strauss, "Algorithms for simultaneous sparse approximation. Part I: Greedy pursuit," *Signal Processing*, vol. 86, no. 3, pp. 572–588, 2006.